Chapter 3.

γ-ray irradiation induced mechanical study of WS_2 nanosystems dispersed in NaCMC polymeric solution

3.1 Introduction

Gamma (γ) ray irradiation, a type of ionizing radiation is an efficient strategy to modify the physical and chemical properties of the nanocomposites. It is a simple, user-friendly and high-purity technique to alter the material properties due to its strong penetration power with ultra-uniformity [1,2]. This ionizing radiation leads to atomic displacement, resulting in the electronic excitation of materials, affecting the vital properties of the structure of the materials [3]. When a material is subjected to γ-irradiation, energy deposits in an explicitly localized region, producing ionization, excitation, and the breakage of chemical bonds, along with the formation of numerous free radical species. Thus, the properties of the materials can be altered through these free radicals by reacting with the nearby elements [4]. Studies have also been carried out to modify the fabricated nanocomposites, filler materials, or raw polymers by employing charge particle irradiation, electron beam, focused ion beam, or UV rays [5]. Recent articles have shown that extensive use of γ-rays can modify the physicochemical properties of 2D nanosystems, thereby promoting chemical reactions to occur on the surfaces [6]. It is an effective technique for altering material morphology and surface structure through the creation of defects, vacancies, dislocations, etc. [7]. There are limited reports on the studies of the effect of γ-ray irradiation on the properties of 2D TMDC systems. In an article, Felix *et al*. reported ferromagnetic hysteresis due to the presence of defect configuration on single-layer WS_2 crystals exposed to 400 Gy γ-dose using ^{60}Co as the source of radiation [8]. Isherwood *et al*. studied the effect of γ-dose after an adsorbed dose of 500 kGy on the MoS_2 system and observed edge-selective etching due to the reduced rate of reaction between the MoS_2 layer and radiolytic adsorbates [9]. In a very recent article by Jadhav *et al.*, γ-irradiation at a dose of 50 kGy and 500 kGy showed a 10- to 100-fold increase in saturation current, exhibiting profound enhancement in the electrical properties of WS_2 material [10].

The addition of TMDC materials like WS_2 into the polymeric matrix can also improve mechanical and electrochemical sensing properties [11,12]. However, the mechanical strength of 2D layered WS_2 nanosystems dispersed in a polymer namely, sodium salt of carboxymethyl cellulose (NaCMC) under radiation exposure has not yet been explored. It was known that NaCMC is a polysaccharide, which is a water-soluble cellulose derivative containing carboxymethyl groups ($-CH_2-COOH$) attached to some of the hydroxyl groups of glucopyranose monomers [13,14]. Cellulose and its derivatives have been increasingly used in various fields, such as corrosion inhibition, due to their eco-friendly, biodegradable nature, etc. As an anionic polyelectrolyte, CMC has also been widely utilized for its colorless and optical transparency, film-forming ability, elasticity and tensile strength, flexibility and resilience, low toxicity and non-allergenic properties, as well as superb hydrophilicity [15,16].

This chapter examines the effects of γ-irradiation on exfoliated WS_2 systems, with doses ranging from 10 kGy to 40 kGy. The irradiation doses in this study were selected within a moderate range of gamma (γ) ray exposure, based on insights gained from previously reported works. For instance, Wu *et al*. utilized a γ-ray dose of 30 kGy to investigate the frictional and electrical properties of the analogous WSe_2 system [17]. In a previous study by our group, a phase transition from hexagonal to trigonal WS_2 was witnessed at a high enough γ-dose of 96 kGy [18]. Furthermore, Li *et al.* noted that mild to moderate γ-irradiation can have beneficial effects on layered graphitic materials [19]. This is particularly relevant, as a higher number of γ-photons would produce a greater density of recoiled electrons, which in turn could lead to increased structural disorder or localized amorphization within the material.

The structural, vibrational, and elemental compositional study of WS_2 after irradiation were analyzed using XRD, Raman, and XPS analysis to understand the effect of γ-photon exposure. Later, the γ-irradiated WS_2 nanosystems were dispersed in a host matrix NaCMC polymeric solutions to make films for mechanical studies. The tensile properties of free-standing WS_2/NaCMC nanocomposite films were investigated before and after irradiation at critical doses of lower (10 kGy) and higher (35 kGy) doses of γ-ray exposure for varied wt.% concentrations.

The exfoliated WS_2 systems were kept in a γ-irradiation chamber available at UGC-DAE CSR, Kolkata, for the irradiation experiment. Here, ^{60}Co was chosen as a source of γ-irradiation, imparting energy of ~1.3 MeV at a dose rate of 1.75 kGy/h under an ambient temperature of ~300 K. The samples were marked for 0 kGy (un-irradiated), 10 kGy, 25 kGy, 30 kGy, 35 kGy, and 40 kGy. The samples were extracted from the chamber after being exposed for the specified duration, offering suitable doses of interest.

3.2 Physical properties of γ-irradiated WS_2/NaCMC films

3.2.1 Structural and vibrational features of γ-irradiated WS_2 nanosystems

The powder X-ray diffraction (XRD) patterns of the un-irradiated and exfoliated sheets of WS_2 exposed to γ-rays with doses between 10-40 kGy can be found in Fig. 3.1(a). The diffraction peaks shown are obtained in the range of Bragg's diffraction angle, 2θ = 10º-70º. The peaks situated at 2θ ~14.6º, 29.05º, 44.25º, and 60.11º corresponded to (002), (004), (006), and (008), respectively and are indexed to the hexagonal crystal structure of WS_2 featuring space group P63/*mmc* in the JCPDS card no. 08-237 [20,21]. The (002) peak appeared to be the preferred orientation of the crystallites, signifying a high degree of crystallinity along the *c*-axis direction (Fig. 3.1(b)). In addition, the lattice parameters, average crystallite sizes, and micro-strains caused by stress resulting from lattice distortions after radiation exposure were estimated by analyzing the XRD patterns, as

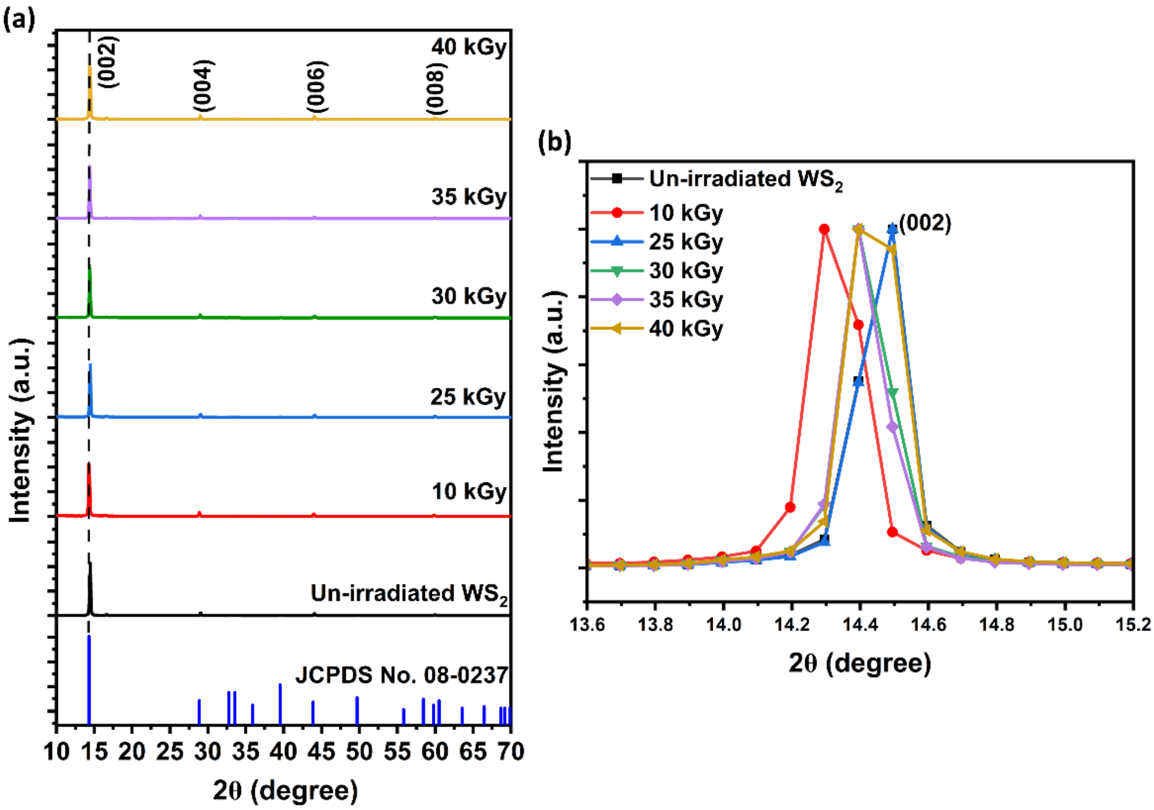

Figure 3.1: (a) Powder XRD patterns of un-irradiated and irradiated WS_2 exposed to 10-40 kGy doses of γ-rays, (b) plots showing the (002) peak oriented along the *c*-axis direction of the hexagonal phase structure of WS_2 system.

Table 3.1. Structural parameters of WS_2 systems upon γ-irradiation at 10-40 kGy.

Sl. No.	**Sample (WS_2)**	**Lattice parameter along *c*-axis (Å)**	**Average crystallite size, d_c (nm)**	**Micro-strain, ε $\times 10^{-3}$**
1	Un-irradiated	12.24	69.9	0.41
2	10 kGy	12.35	46.8	0.74
3	25 kGy	12.24	64.2	0.54
4	30 kGy	12.28	48.2	0.72
5	35 kGy	12.28	49.5	0.70
6	40 kGy	12.26	55.9	0.62

shown in Table 3.1. The crystallite sizes, exhibiting anomalous variations, were observed to decrease when exposed to high-energy γ-photons, reducing from ~70 nm to as small as ~47 nm within the dose range of 10-40 kGy. Slightest alteration in lattice constant, but an observable change in average crystallite sizes can be found with an increase in γ-dose. Due to high-energy γ-irradiation, which ionizes the atomic or molecular sub-lattices of the system under study, ample point defects or vacancies are likely to form. It is worth mentioning here that, atomic masses of the corresponding constituents and radiation dose would play a decisive role in modifying the structure of the WS_2 system [22]. The accumulation of irradiation-induced defects leads to lattice distortions and a slight expansion of the crystal structure, shifting the XRD peaks toward lower Bragg angles with increasing γ-dose. The non-uniform distribution of these distortions contributes to peak broadening, signifying the development of micro-strain within the irradiated material. At higher doses, these deformations or defects increase the internal stress locally, influencing the lattice structure and diminishing the crystallites into smaller ones. However, the effect follows an anomalous trend. These anomalous variations indicate competing events occurring due to γ-irradiation, leading to the accumulation of defects on the surface of WS_2 layers, fragmentation, and recrystallization of grains at comparatively higher doses.

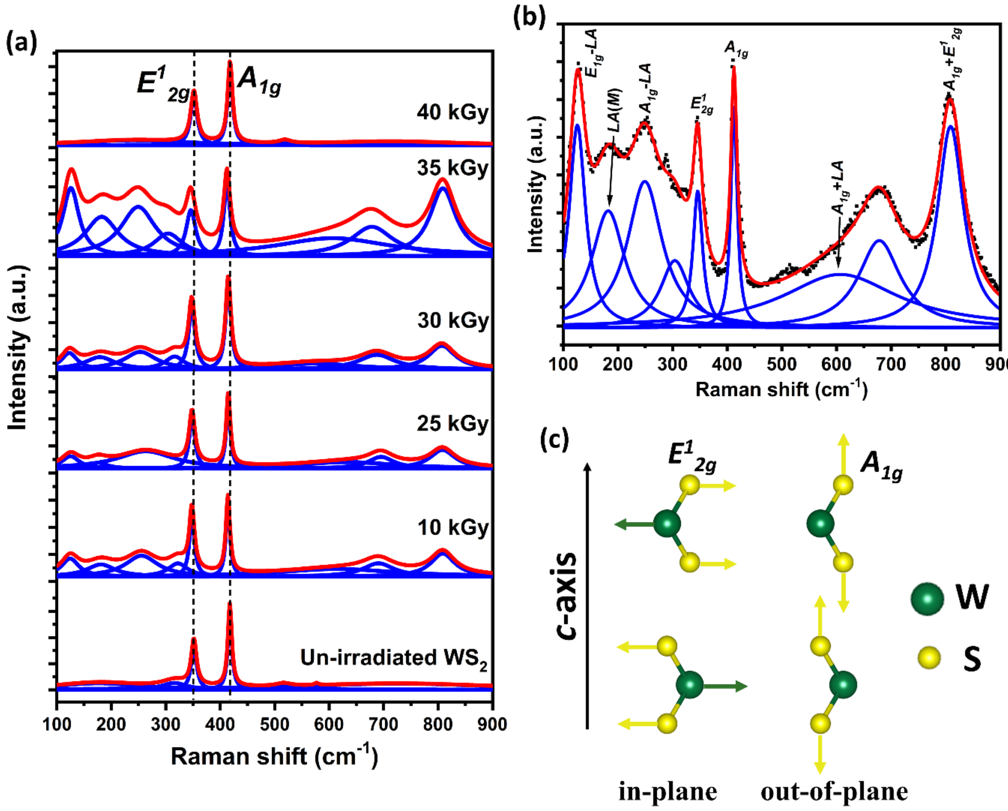

Figure 3.2: (a) Raman spectra of un-irradiated WS_2 and WS_2 irradiated with γ-ray exposure varied at doses from 10-40 kGy along with multi-peak Lorentzian fit, (b) deconvoluted Raman spectra at 35 kGy with second-order Raman modes due to irradiation effect, (c) schematic representation of the direction of the in-plane ($E^1{}_{2g}$) and out-of-plane (A_{1g}) vibrational modes.

The Raman spectra of the un-irradiated WS_2 and irradiated with γ-rays at varied doses of γ-rays of 10 kGy, 25 kGy, 30 kGy, 35 kGy and 40 kGy, respectively, plotted with multi-peak Lorentzian fittings are shown in Fig. 3.2. The intense in-plane ($E^1{}_{2g}$) and out-of-plane (A_{1g}) first-order Raman modes emerge at 352 cm^{-1} and 418 cm^{-1}, respectively (Fig. 3.2(a)). Additionally, the well-resolved Raman spectra in the case of 35 kGy reveal the evolution of second-order Raman signatures due to radiation exposure. These peaks were attributed to the E_{1g} *-LA,* A_{1g} *- LA*, A_{1g} *+ LA, 4LA* and $A_{1g} + E^1{}_{2g}$ modes appearing at ~128 cm^{-1}, 248 cm^{-1}, 606 cm^{-1}, 678 cm^{-1}, and 808 cm^{-1}, respectively (Fig. 3.2 (b)) [21,23]. The peak revealed at ~178 cm^{-1} is attributed to the *LA(M)* mode, indicating the presence of defects in the WS_2 system that have become more prominent after irradiation at a dose range of 10-35 kGy [24,25]. Moreover, the intensity ratios were calculated considering the $E^1{}_{2g}$ and A_{1g} modes in the Raman spectra for varied doses of γ-irradiation. The highest ratio, ~0.79, observed at the first dose shown in Table 3.2, indicates radiation-assisted exfoliation in the layered WS_2 system. At higher doses, the γ-irradiation predominantly

Table 3.2. Raman modes identification and intensity ratios were investigated from the acquired Raman spectra.

Sl. No.	Sample (exfoliated WS_2)	Peak position (cm^{-1})		E^1_{2g}/A_{1g} (Intensity ratio)
		E^1_{2g} mode	A_{1g} mode	
1	0 kGy	352	418	0.55
2	10 kGy	348	414	0.79
3	25 kGy	349	414	0.72
4	30 kGy	347	414	0.70
5	35 kGy	347	412	0.50
6	40 kGy	352	418	0.63

induces chalcogen vacancies, leading to a decrease in the intensity up to 35 kGy, possibly due to the disruption of bonds between the tungsten (W) and sulfur (S) atoms. Again, at the maximum dose of 40 kGy, a structural rearrangement of atoms would occur, causing the E^1_{2g}-to-A_{1g} intensity ratio to augment again.

3.2.2 Elemental compositional analysis

The elemental compositions and chemical state of un-irradiated and γ-irradiated WS_2 systems were investigated using an XPS study, shown in Fig. 3.3. The XPS survey scans of un-irradiated WS_2 and after γ-irradiation at 10 kGy and 35 kGy can be found in Fig. 3.3(a). The presence of W 4*f* and S 2*p* core-level spectra was confirmed in the survey spectra of WS_2 systems. In addition, binding energy peaks corresponding to C 1*s*, N 1*s*, and O 1*s* could be observed due to environmental contaminants or during sample processing. From the W 4*f* core level spectra, the resolved plots of W 4*f* core level spectra display doublet species, W $4f_{7/2}$ and W $4f_{5/2}$ states of tungsten species, resulting in peaks at ~32.4 eV and ~34.6 eV, respectively. A broad peak at around ~37.8 eV represents the W $5p_{3/2}$ state of tungsten shown in Fig. 3.3(b) [26]. We can observe minute shifting in the W $4f_{7/2}$ states by ~0.1 eV and ~0.3 eV towards lower binding energy at low and higher doses of γ-ray irradiation, respectively, along with a shift in the W $4f_{5/2}$ states by ~0.1 eV and ~0.2 eV. Thus, these peaks belong to the W^{4+} oxidation state of the 2*H*-WS_2 phase. Additionally, a small shoulder peak appears at around 35.8 eV, corresponding to the W-O bond and indicative of the W^{6+} oxidation state [27]. This peak associated with W-O reduces

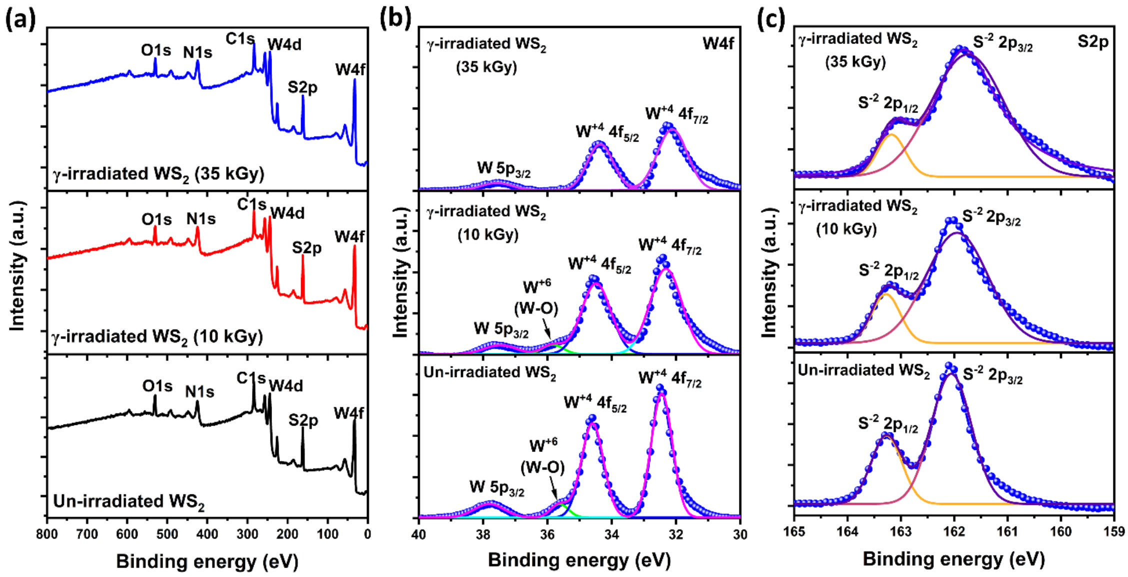

Figure 3.3: (a) XPS survey scan, (b) W 4*f*-core level spectra, (c) S 2*p*-core level of un-irradiated and γ-irradiated WS_2 at 10 kGy and 35 kGy, respectively.

with γ-irradiation and completely disappears at a high γ-dose of 35 kGy, owing to changes in the chemical environment of the WS_2 systems. Furthermore, the resolved plots of S 2*p* core-level spectra reveal peaks at ~162.1 eV and ~ 163.3 eV ascribed to S $2p_{3/2}$ and S $2p_{1/2}$ states of divalent sulfide ions (S^{2-}) of un-irradiated WS_2 (Fig. 3.3(c)) [28,29]. Similarly, peaks were observed in γ-irradiated WS_2 systems at different doses of 10 kGy and 35 kGy, with a slight shift toward lower binding energies in the S $2p_{3/2}$ states by ~0.1 eV and ~0.3 eV, respectively. This shift in the W 4*f* and S 2*p* core level spectra indicates a sulfur deficiency, and thus, reduced to WS_{2-x} phase as a result of γ-irradiation [30]. Moreover, a decrease in the peak intensity as well as broadening in the core-level spectra of W 4*f* and S 2*p* with radiation exposure further advocates variations in the atomic compositions in the WS_2 system due to *γ*-impact [31]. The dislodgment of atoms in the structurally ordered lattice, with sulfur vacancies being the most probable event that would lead to the suppressed peak intensity in the core-level spectra.

3.3 Mechanical properties of γ-irradiated exfoliated WS_2 dispersed in NaCMC

3.3.1 Load bearing capacity, elasticity, and breaking points

The tensile properties of γ-irradiated WS_2 nanosystems were studied by dispersing them in the NaCMC polymeric host matrix. Both wt.% and γ-dose aspects have been considered independently while acquiring data. To attain superior mechanical properties for the WS_2 nanosheets, adequate interfacial interaction between the nanosheets and the host matrix is essential. Consequently, the homogenous dispersion of the nanosheets in the matrix plays a vital role. The polymeric composites containing γ-irradiated WS_2 systems were developed to form nanocomposite films and subsequently studied using stress-strain curves, shown in Fig. 3.4(a-c). The stress-strain curves acquired can essentially be divided into two distinct segments: (a) the elastic, and (b) the plastic regions. The elastic region spans a strain range of approximately 40-80% based on the sample specimen, un-irradiated, or irradiated with γ-dose, and with the extent of loading. Beyond this linear region, plastic deformation occurs and is characterized by strain hardening. This plastic regime follows a growing trend independently. Herein, a comparable elongation percentage occurs for a higher amount of tensile stress, and upon achieving maximum strain, the breaking point is attained.

Moreover, corresponding to different strain values, there is a slight change in the stress level of the irradiated WS_2 systems subjected to γ-ray exposure of 10 kGy and 35 kGy and at a loading of 0.5 wt.% as compared to their un-irradiated counterpart. Specifically, the elongation at break was seen declining with increasing irradiation dose. Further, at 1 wt.% and 5 wt.% of WS_2 loading, there is an anomalous increase in the magnitude of the stress in the irradiated cases of 10 kGy and 35 kGy. This signifies that ultimate tensile strength increases with higher breaking stress for irradiated systems with an augment of WS_2 loading in the NaCMC host matrix at 1 wt.% and 5 wt.% offering respective augments of 83%, and 45% eventually. A substantial enhancement in the ultimate tensile strength could be observed from the stress-strain curve in the case of 1 wt.% WS_2/NaCMC nanocomposite system compared to the pure NaCMC (included in *Appendix* (Fig. A1)) and at a lower γ-dose of 10 kGy. The better reinforcement ability of WS_2 as a filler material in the NaCMC polymeric host matrix at 1 wt.%, together with better interfacial interaction, is expected to enhance the tensile property at large [32,33]. This also implies an effective transfer and load-bearing capacities of the nanocomposites due to an adequate filler distribution within the polymeric matrix. In addition, the large surface area of the WS_2 nanosheets used as nanofillers plays a crucial role in determining the mechanical properties of the nanocomposite systems. However, at higher loading concentrations, agglomeration and re-stacking of sheets due to van der Waal interaction between the layers would lower the surface area, and the interfacial interaction between the guest WS_2 and the host matrix of NaCMC [34,35]. As a result, the tensile strength at

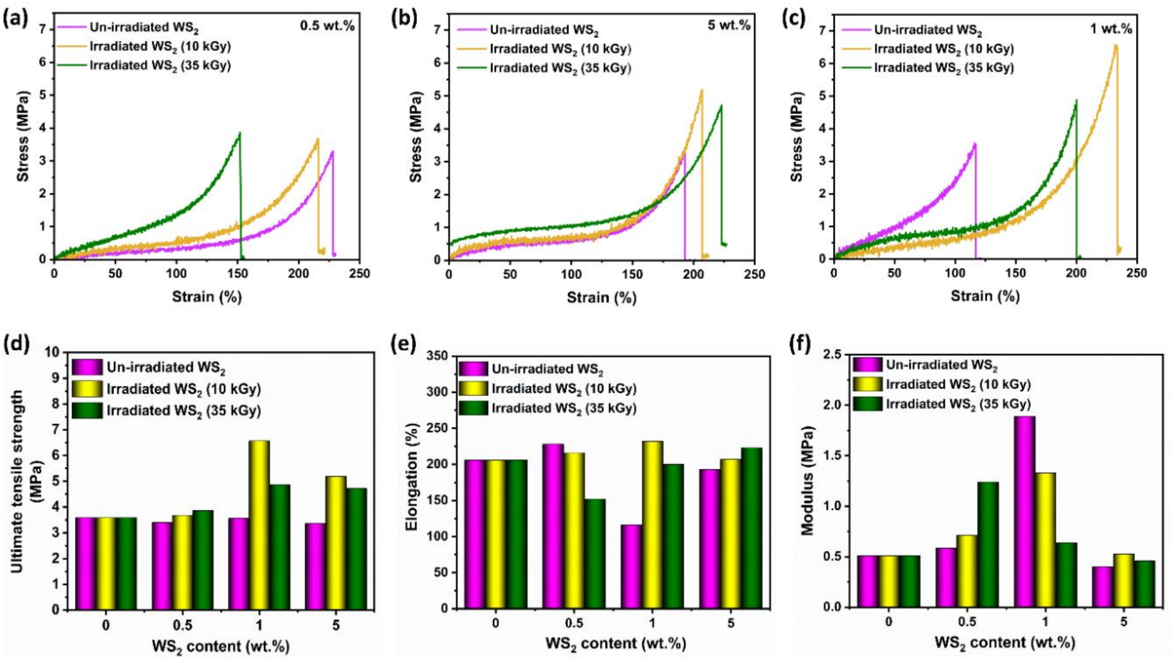

Figure 3.4: Mechanical stress *vs*. strain plot at a strain rate of 5 mm/min of WS_2/NaCMC nanocomposite films plotted for (a) 0.5 wt.%, (b) 1 wt.% and (d) 5 wt.% of un-irradiated WS_2, and γ-irradiated WS_2 at 10 kGy, 35 kGy, respectively. A comparative view of un-irradiated and irradiated WS_2 at 10 kGy and 35 kGy to variation in (d) ultimate tensile strength (MPa), (e) elongation at break (%), and (f) Young's modulus (MPa) with varied concentrations of WS_2 content in wt.% are shown.

higher γ-doses of WS_2 nanosheets gets lowered. A comparison of un-irradiated and irradiated WS_2 at doses of 10 kGy and 35 kGy is presented, highlighting the changes in ultimate tensile strength (MPa), elongation at break (%), and modulus (MPa) across various WS_2 content in wt.% (Fig. 3.4(d-f) & Table 3.3). The elongation at break was maximum (up to ~228%) in the un-irradiated case and for the lower loading level (0.5 wt.%) of WS_2 content. With higher loadings of WS_2, such as 1 wt. % and 5 wt.%, the elongation at break shows up for irradiated cases at 10 kGy and 35 kGy of γ-ray exposure. This signifies that the specimen tends to become ductile after being exposed to γ-dose, and was more prominent at higher loadings of WS_2 content. Consequently, the mechanical properties exhibited an enhanced tensile strength, ductility, and flexibility for 1 wt.% of WS_2/NaCMC nanocomposite film, considering WS_2 at a γ-dose of 10 kGy. It is imperative to note that, due to uneven solvent drying, slight variations in film thickness might occur during the solvent evaporation process.

Table 3.3. Parameters related to the mechanical properties of WS_2/NaCMC composites using un-irradiated (0 kGy) and γ-irradiated (at 10 kGy and 35 kGy) WS_2 fillers at varied loading wt.% in the polymer.

Sl. No.	**Samples**	**Ultimate tensile stress (MPa)**			**Elongation (%)**			**Youngs modulus (MPa)**		
		0 kGy	**10 kGy**	**35 kGy**	**0 kGy**	**10 kGy**	**35 kGy**	**0 kGy**	**10 kGy**	**35 kGy**
1	0.5 wt.% WS_2/NaCMC	3.4	3.68	3.87	228	216	152	0.584	0.711	1.24
2	1 wt.% WS_2/NaCMC	3.56	6.57	4.87	116	232	200	1.89	1.33	0.638
3	5 wt.% WS_2/NaCMC	3.36	5.19	4.72	193	207	223	0.401	0.526	0.458

An unusual trend in stress-strain response was observed in the case of un-irradiated WS_2 at 1 wt.%, leading to a higher modulus value of 1.89 MPa, making the composite stiffer. However, the stiffness remained insensitive to the strain rates after *γ*-ray exposure. The γ-irradiation creates vacancies or point defects and promotes atomic reorganization locally. Here, we speculate structural reordering with defect manifestation that would account for interconnected structures within the cellulose host matrix. Nevertheless, when the dose range increases significantly, an increase in internal stress can cause lattice distortion, resulting in agglomeration of sheets, thereby disrupting the interfacial growth of WS_2 nanofiller and host matrix [19].

Additionally, the Young's modulus (initial elastic slope), which reflects the material's initial elastic stiffness, exhibits minimal variation across the applied strain range with irradiation. To be mentioned, *γ*-irradiation is known to induce structural changes in the WS_2 system, such as bond weakening and lattice distortion, which can contribute to a reduction in modulus under certain conditions. Nonetheless, factors like the presence of microcracks, voids, and the uneven clustering of WS_2 nanofillers may contribute to a reduction in modulus. The reason behind these features could be understood through the morphological analysis of the fractured surfaces of the WS_2/NaCMC nanocomposite films discussed in the next section.

3.3.2 Reinforcement mechanisms of the fractured surfaces

The morphological analysis of the fractured surfaces and their reinforcement mechanisms developed in the WS_2/NaCMC composite films are shown through the FE-SEM images. The morphological features of pure NaCMC and exfoliated thinner nanosheets before being exposed to γ-irradiation can be found in Fig. 3.5. The exfoliated sheets possess a layered morphology that has a large surface area and lateral diameters of ~1-2 μm. The fractured structures of the composite systems show ample rough surfaces, indicating ductile failure in the tensile test [36]. The morphological features of un-irradiated WS_2 before and after tensile load are shown in Fig. 3.6. The microstructure of 1 wt.% WS_2/NaCMC nanocomposite films before and after the tensile test show some interconnected patterns due to the percolation of polymeric cellulose into the associated gaps of WS_2 nanosheets (Fig. 3.7 A(a,b)). These films displayed tightly packed structures with no visible voids, microcracks, or signs of interfacial debonding on the surface, indicating adequate adhesion between the matrix and the filler. The surface morphology

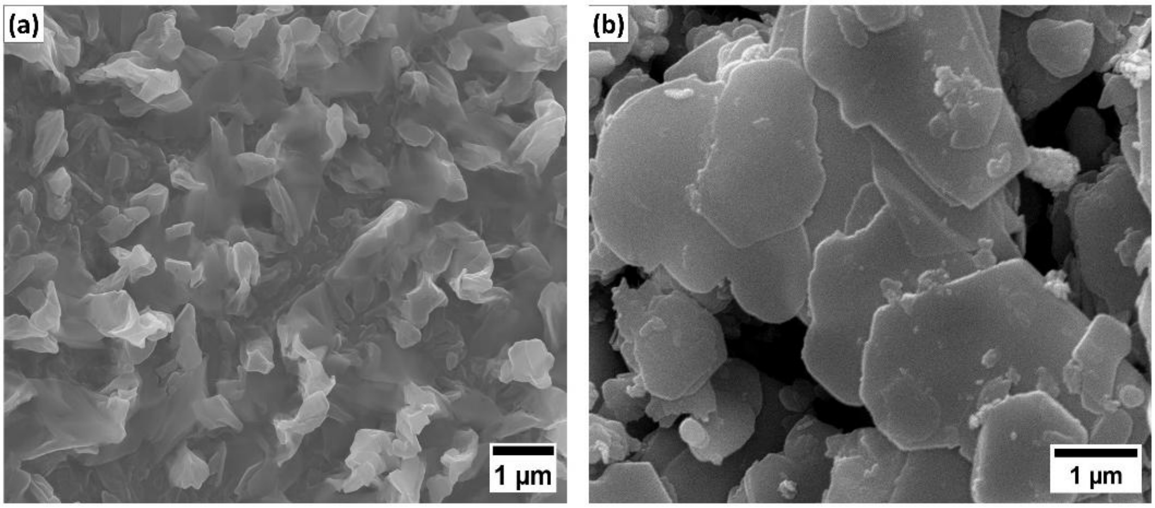

Figure 3.5: FE-SEM images of (a) pure NaCMC film and (b) exfoliated WS_2 nanosheets without NaCMC.

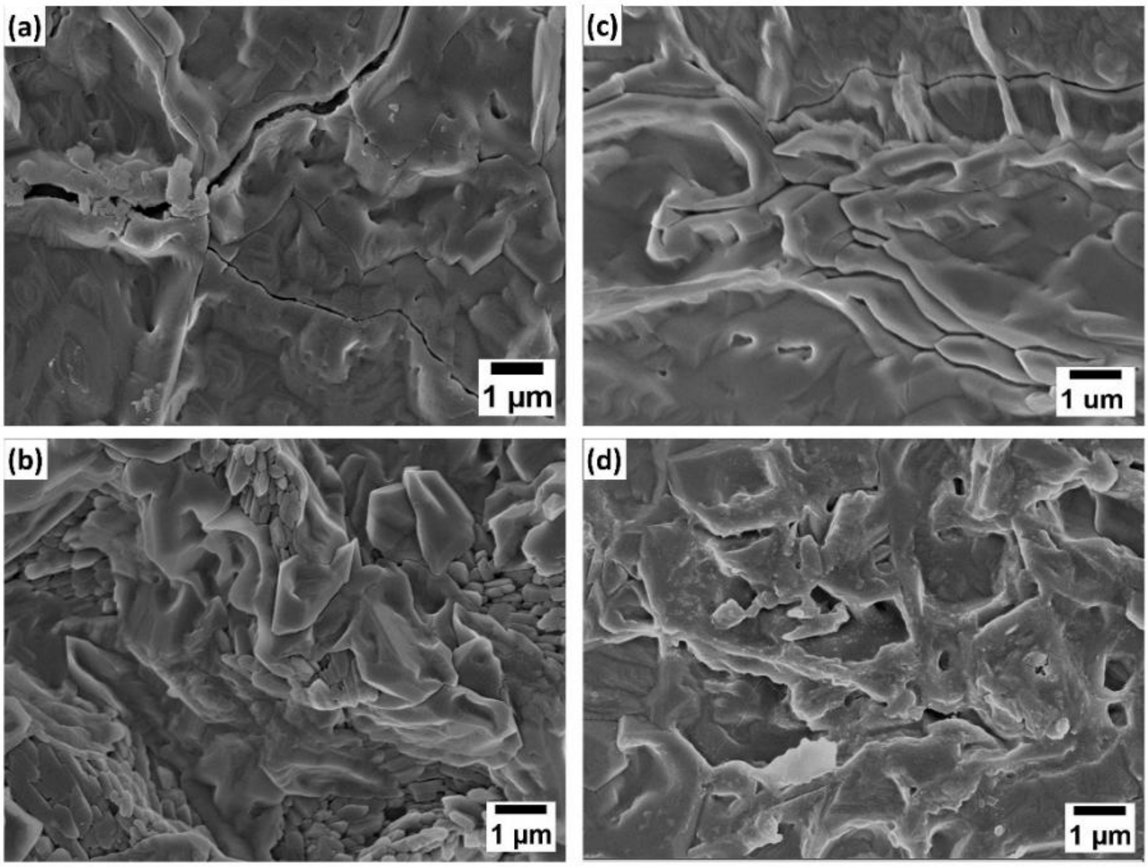

Figure 3.6: FE-SEM images of un-irradiated WS_2/NaCMC (upper panel) before stress is applied and (lower panel) with strain, i.e. after stress is released, respectively for (a,b), 1 wt.%, (c,d) 5 wt.% loading of WS_2.

also lacked large agglomerates, further suggesting adequate dispersion and interfacial compatibility. These microstructures between the polymer and WS_2 nanofillers contributed to the enhanced tensile strength observed at a γ-dose of 10 kGy. These structured networks also played a role in enduring crack propagation in the material, thus improving mechanical strength. Notably, the WS_2/NaCMC nanocomposite films irradiated at 10 kGy, particularly with 1 wt.% loading, exhibited a significant augment in energy absorption capacity and the area under the stress-strain curves at higher strain rates, featuring a more ductile response [37].

At a higher *γ*-dose of 35 kGy, the tensile strength decreased compared to that at 10 kGy. This reduction was attributed to radiation-induced micro-damage, where lattice distortions led to increased internal stress, creating voids within the material structure [38]. These structural changes led to the clumping of WS_2 at 1 wt.%, adversely affecting the mechanical performance. At 5 wt.%, microcracks have evolved in the WS_2/NaCMC

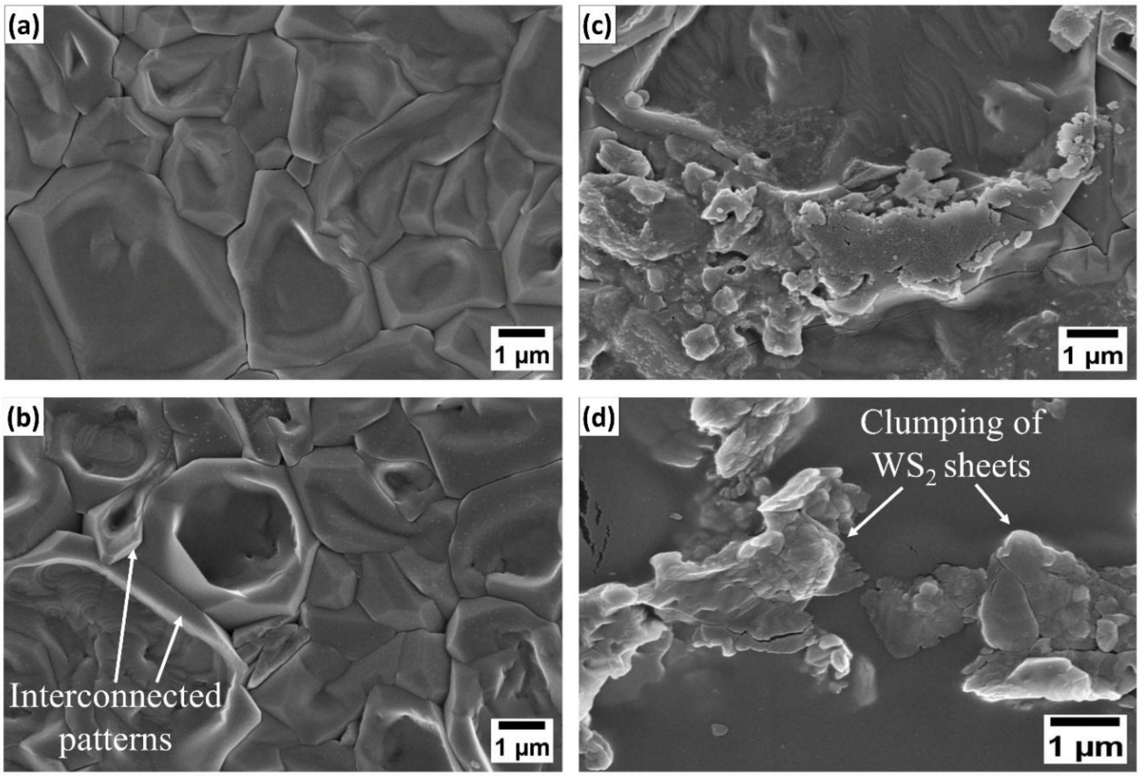

Figure 3.7 (A). FE-SEM images of the reinforcement mechanisms developed in 1 wt.% WS_2/NaCMC nanocomposite films, before (upper panel) and after (lower panel) applying strain, respectively, upon exposure to γ-rays at (a,b) 10 kGy, and (c,d) 35 kGy.

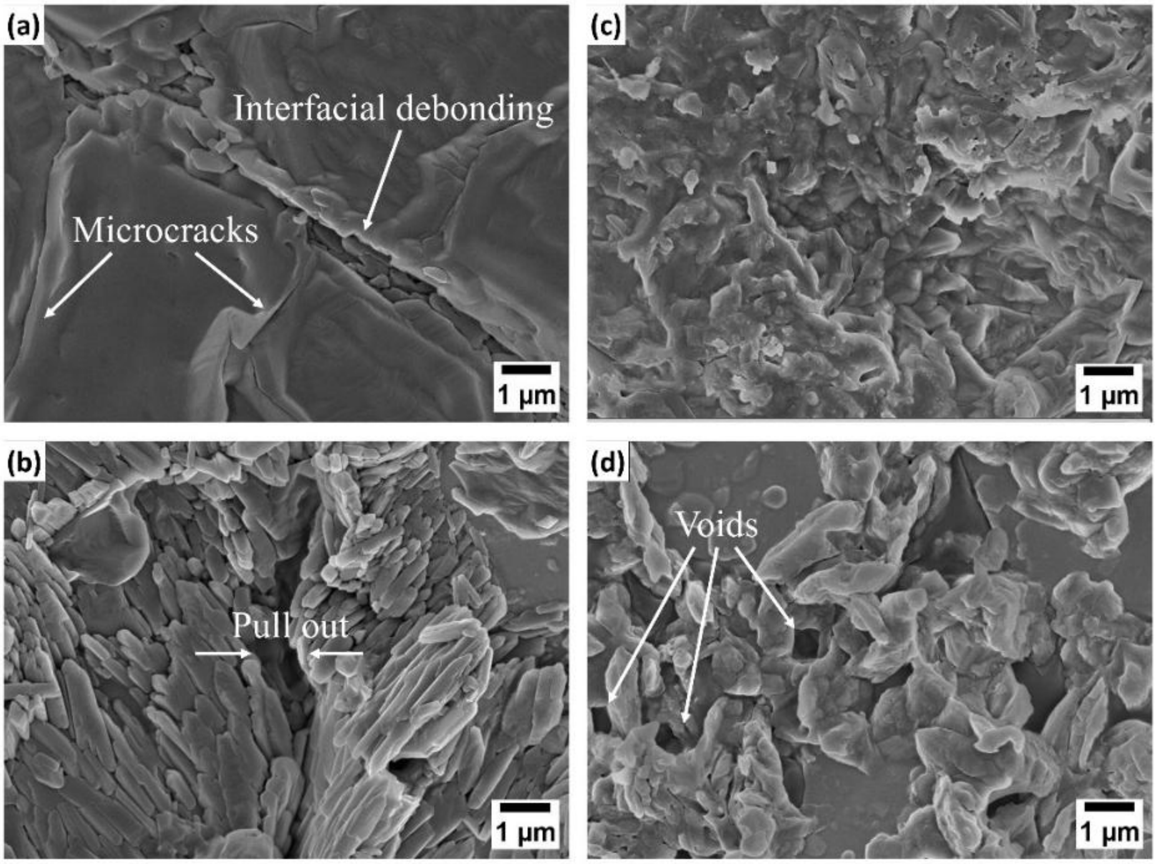

Figure 3.7 (B): FE-SEM images of the reinforcement mechanisms developed in 5 wt.% WS_2/NaCMC nanocomposite films, before (upper panel) and after (lower panel) applying strain, respectively, upon exposure to γ-rays at (a,b) 10 kGy, and (c,d) 35 kGy.

composite films of 10 kGy *γ*-dose. This was primarily driven by micro-damage mechanisms such as crack propagation and interfacial debonding. These were likely to be due to stress concentrations caused by interfacial voids and cracks around micron-sized filler material that appeared in the form of elongated structures within the polymeric NaCMC matrix, observed in Fig. 3.7 B(a,b). Such microcracks led to the collapse of the interconnected microstructures, ultimately resulting in reduced mechanical strength [39]. This is an intrinsic toughening mechanism developed to improve the fracture resistance of low-toughness materials. In addition, it signifies poor interfacial bonding at the interface [40]. Thus, crack propagation, interfacial debonding and pull-out of fractured WS_2 nanosheets mostly contribute to the fracture toughness of the nanocomposites. Moreover, the surface structures of higher doses of *γ*-rays display complex textures with irregular patterns across their entire surface, resulting in voids and cracks in their microstructure due to clustering of WS_2 sheets in the case of 1 wt.% and 5 wt.% cases (Fig. 3.7 A (c,d) and

Fig. 3.7 B (c,d)). As a result, the tensile strength at a 35 kGy dose was comparatively lower than that at a 10 kGy dose. Thus, the mechanical properties of WS_2/NaCMC nanocomposite films are significantly influenced by the type of irradiation dose considered, and consequently, by the morphological evolution, defect formation, and stress accumulation in the system under study [41].

3.4 Concluding remarks

In conclusion, this chapter explores the mechanical properties of WS_2/NaCMC nanocomposite systems following γ-ray exposure to exfoliated WS_2 systems. Before analysing these properties, a structural study was conducted on the WS_2 system both before and after irradiation, without incorporating it into the NaCMC matrix. Here, the XRD analysis confirms that WS_2 has a hexagonal phase structure (*P63/mmc* space group) and is oriented along the *c*-axis. Raman spectroscopy reveals mixed modes in γ-irradiated WS_2, with first-order Raman modes appearing at 352 cm^{-1} (E^1_{2g} mode) and 418 cm^{-1} (A_{1g} mode). Additionally, prominent defect-mediated *LA* modes emerge near 178 cm^{-1}, particularly at a γ-dose of 35 kGy. The XPS analysis of the W 4*f* and S 2*p* core-level spectra indicates that exfoliated WS_2 retains its 2*H* phase with W^{4+} and S^{2-} oxidation states. Moreover, γ-ray exposure leads to peak broadening and reduced intensity in the core-level spectra of W 4*f* and S 2*p* compared to un-irradiated WS_2, suggesting structural modifications.

As for the mechanical study, stress-strain analysis was conducted, revealing an elastic strain range of around 40-80%, depending on the nature of WS_2 loading and γ-ray dose. Beyond this range, plastic deformation occurs, exhibiting strain-hardening before failure. The ultimate tensile strength increases with higher WS_2 nanofiller loadings, as can be observed in irradiated systems. Specifically, WS_2/NaCMC nanocomposites offer an increase in tensile strength up to 83% and 45% at 1 wt.% and 5 wt.%, respectively. Notably, mechanical properties, including tensile strength, ductility, and flexibility, are significantly enhanced at 1 wt.% of the composites, particularly at a γ-dose of 10 kGy. Thus, irradiation alters the lattice structure of materials, enhancing the transfer efficiency and interfacial bonding between WS_2 nanofillers and the NaCMC polymer matrix at low doses.

However, microstructural analysis reveals the formation of microcracks and stress concentration zones in the WS_2/NaCMC composites, particularly at higher nanofiller loadings and radiation doses. These suggest that while low-dose γ-radiation can enhance tensile properties, excessive exposure may lead to increased internal stress, lattice distortions, and structural defects. This, in turn, promotes agglomeration and void formation, ultimately diminishing the mechanical performance of the composites.

References

[1] Chen, R. S., Ab Ghani, M. H., Ahmad, S., Tarawneh, M. A., Gan, S. Tensile, thermal degradation and water diffusion behaviour of gamma-radiation induced recycled polymer blend/rice husk composites: Experimental and statistical analysis. *Composites Science and Technology*, *207*: 108748, 2021.

[2] Salari, M., Sowti Khiabani, M., Rezaei Mokarram, R., Ghanbarzadeh, B., Samadi Kafil, H. Use of gamma irradiation technology for modification of bacterial cellulose nanocrystals/chitosan nanocomposite film. *Carbohydrate Polymers*, *253*: 117144, 2021.

[3] Walker, R. C., Shi, T., Silva, E. C., Jovanovic, I., Robinson, J. A. Radiation effects on two-dimensional materials. *Physica status solidi (a)*, *213*(12): 3065–3077, 2016.

[4] Tarawneh, M. A., Saraireh, S. A., Chen, R. S., Ahmad, S. H., Al- Tarawni, M. A. M., Yu, L. J. Gamma irradiation influence on mechanical, thermal and conductivity properties of hybrid carbon nanotubes/montmorillonite nanocomposites. *Radiation Physics and Chemistry*, *179:* 109168, 2021.

[5] Chmielewski, A. G., Chmielewska, D. K., Michalik, J., Sampa, M. H. Prospects and challenges in application of gamma, electron and ion beams in processing of nanomaterials. *Nuclear Instruments and Methods in Physics Research Section B: Beam Interactions with Materials and Atoms*, *265*(1): 339–346, 2007.

[6] Ansón-Casaos, A., Puértolas, J.A., Pascual, F.J., Hernández-Ferrer, J., Castell, P., Benito, A.M., Maser, W.K., Martínez, M.T. The effect of gamma-irradiation on few-layered graphene materials. *Applied Surface Science*, *301*: 264–272, 2014.

[7] Majhi, S. M., Mirzaei, A., Navale, S., Kim, H. W., Kim, S. S. Boosting the sensing properties of resistive-based gas sensors by irradiation techniques: a review. *Nanoscale*, *13*(9): 4728–4757, 2021.

[8] Felix, J.F., Da Silva, A.F., da Silva, S.W., Qu, F., Qiu, B., Ren, J., De Azevedo, W.M., Henini, M., Huang, C.C. A comprehensive study on the effects of gamma radiation on the physical properties of a two-dimensional WS_2 monolayer semiconductor. *Nanoscale Horizons*, *5*(2): 259–267, 2020.

[9] Isherwood, L. H., Athwal, G., Spencer, B. F., Casiraghi, C., Baidak, A. Gamma radiation-induced oxidation, doping, and etching of two-dimensional MoS_2 crystals. *The Journal of Physical Chemistry C*, *125*(7): 4211–4222, 2021.

[10] Jadhav, P. R., Kolhe, P. T., Ghemud, V. S., Shelke, P. N., Patole, S. P., Dhole, S. D., Dahiwale, S. S. Modification of WS_2 thin film properties using high dose gamma irradiation. *Nanotechnology*, *35*(33): 335701, 2024.

[11] Rana, S., Singh, V., Singh, B. Recent trends in 2D materials and their polymer composites for effectively harnessing mechanical energy. *iScience*, *25*(2): 103748, 2022.

[12] Sanyal, G., Jaiswal, R., Chakraborty, B. 11 - 2D materials-conducting polymers-based hybrids for electrochemical sensing. In C. S. Rout (Ed.), *2D Materials-Based Electrochemical Sensors*, pages 325–354, ISBN:978-0-443-15293-1, Elsevier, 2023.

[13] Keller, J. D. Sodium carboxymethylcellulose (CMC). In *Food hydrocolloids*, pages 43–109, CRC Press, 2020.

[14] Lopez, C. G., Rogers, S. E., Colby, R. H., Graham, P., Cabral, J. T. Structure of sodium carboxymethyl cellulose aqueous solutions: A SANS and rheology study. *Journal of Polymer Science Part B: Polymer Physics*, *53*(7): 492–501, 2015.

[15] Al Kiey, S. A., Hasanin, M. S., Dacrory, S. Potential anticorrosive performance of green and sustainable inhibitor based on cellulose derivatives for carbon steel. *Journal of Molecular Liquids*, *338:* 116604, 2021.

[16] Inagamov, S. Y., Asrorov, U. A., Xujanov, E. B. Structure and physico-mechanical properties of polyelectrolyte complexes based on sodium carboxymethylcellulose polysaccharide and polyacrylamide. *East European Journal of Physics*, (4): 258–266, 2023.

[17] Wu, X., Zheng, X., Zhang, G., Dong, H., Chen, X. Influences of thickness and gamma-ray irradiation on the frictional and electronic properties of WSe_2 nanosheets. *AIP Advances*, *11*(4): 045229, 2021.

[18] Sarmah, H. J., Mohanta, D., Saha, A. Perceptible exciton-to-trion conversion and signature of defect mediated vibronic modes and spin relaxation in nanoscale WS_2 exposed to γ-rays. *Nanotechnology*, *31*(28): 285706, 2020.

[19] Li, B., Feng, Y., Ding, K., Qian, G., Zhang, X., Zhang, J. The effect of gamma ray irradiation on the structure of graphite and multi-walled carbon nanotubes. *Carbon*, *60:* 186–192, 2013.

[20] Yan, J., Lian, S., Cao, Z., Du, Y., Wu, P., Sun, H., An, Y. CVD controlled preparation and growth mechanism of 2H-WS_2 nanosheets. *Vacuum*, *207:* 111564, 2023.

[21] Mohan, V. V, Manuraj, M., Anjana, P. M., Rakhi, R. B. WS_2 nanoflowers as efficient electrode materials for supercapacitors. *Energy Technology*, *10*(3): 2100976, 2022.

[22] Pelizzo, M.G., Corso, A.J., Santi, G., Hübner, R., Garoli, D., Doyle, D., Lubin, P., Cohen, A.N., Erlikhman, J., Favaro, G., Bazzan, M. Dependence of the damage in optical metal/dielectric coatings on the energy of ions in irradiation experiments for space qualification. *Scientific Reports*, *11*(1): 3429, 2021.

[23] Rawat, S., Bamola, P., Bisht, M., Bhandari, B. S., Dwivedi, C., Sharma, H. Temperature dependence Raman spectroscopy studies of CVD grown few layer MoS_2 triangular domains. *Materials Today: Proceedings,* 2023.

[24] Aryeetey, F., Ignatova, T., Aravamudhan, S. Quantification of defects engineered in single layer MoS_2. *RSC Advances*, *10*(39): 22996–23001, 2020.

[25] Gontijo, R.N., Zhang, T., Fujisawa, K., Elías, A.L., Pimenta, M.A., Righi, A., Terrones, M., Fantini, C. Multiple excitations and temperature study of the disorder-induced Raman bands in MoS_2. *2D Materials*, *8*(3): 035042, 2021.

[26] Jha, R. K., Nanda, A., Bhat, N. Ultrasonication assisted fabrication of a tungsten sulfide/tungstite heterostructure for ppb-level ammonia detection at room temperature. *RSC advances*, *10*(37): 21993–22001, 2020.

[27] Loh, T. A. J., Chua, D. H. C., Wee, A. T. S. One-step Synthesis of Few-layer WS_2 by Pulsed Laser Deposition. *Scientific Reports*, *5*(1): 18116, 2015.

[28] Urbanová, V., Lazar, P., Antonatos, N., Sofer, Z., Otyepka, M., Pumera, M. Positive and Negative Effects of Dopants toward Electrocatalytic Activity of MoS_2 and WS_2: Experiments and Theory. *ACS Applied Materials & Interfaces*, *12*(18): 20383–20392, 2020.

[29] Lei, T., Chen, W., Huang, J., Yan, C., Sun, H., Wang, C., Zhang, W., Li, Y., Xiong, J. Multi-functional layered WS_2 nanosheets for enhancing the performance of lithium–sulfur batteries. *Advanced Energy Materials*, *7*(4): 1601843, 2017.

[30] Kastl, C., Koch, R.J., Chen, C.T., Eichhorn, J., Ulstrup, S., Bostwick, A., Jozwiak, C., Kuykendall, T.R., Borys, N.J., Toma, F.M., Aloni, S. Effects of Defects on Band Structure and Excitons in WS_2 Revealed by Nanoscale Photoemission Spectroscopy. *ACS Nano*, *13*(2): 1284–1291, 2019.

[31] Sundberg, J., Lindblad, R., Gorgoi, M., Rensmo, H., Jansson, U., Lindblad, A. Understanding the effects of sputter damage in W–S thin films by HAXPES. *Applied Surface Science*, *305*: 203–213, 2014.

[32] Sudarsanam, S. K., Panneerselvam, K. Mechanical and thermal investigation of high-density polyethylene/multi-walled carbon nanotube/tungsten disulfide hybrid composites. *Iranian Polymer Journal*, *33*(8): 1–15, 2024.

[33] Koteswararao, J., Satyanarayana, S. V., Madhu, G. M., Venkatesham, V. Estimation of structural and mechanical properties of Cadmium Sulfide/PVA nanocomposite films. *Heliyon*, *5*(6): e01851, 2019.

[34] Yuan, X. Y., Zou, L. L., Liao, C. C., Dai, J. W. Improved properties of chemically modified graphene/poly (methyl methacrylate) nanocomposites via a facile in-situ bulk polymerization. *Express Polymer Letters*, *6*(10): 847-858, 2012.

[35] Raza, H., Aized, T., Khan, M. B., Imran, M. Tensile testing of polystyrene graphene 2D nano composite membrane. *The International Journal of Advanced Manufacturing Technology*, *94:* 4343–4349, 2018.

[36] Sudarsanam, S. K., Panneerselvam, K. Mechanical and thermal investigation of high-density polyethylene/multi-walled carbon nanotube/tungsten disulfide hybrid composites. *Iranian Polymer Journal*, *33*(8): 1075–1089, 2024.

[37] Cui, J., Wang, S., Wang, S., Li, G., Wang, P., Liang, C. The effects of strain rates on mechanical properties and failure behavior of long glass fiber reinforced thermoplastic composites. *Polymers*, *11*(12): 2019, 2019.

[38] Zhang, X., Hao, L., Liu, X., Niu, M., Shen, S., Wang, S., Fu, E. Radiation effects on microstructure and hardening behavior in high-entropy fiber strengthened Al-based alloy. *Journal of Alloys and Compounds*, *1034*: 181244, 2025.

[39] Shen, H., Wu, Z., Dou, R., Jiao, L., Chen, G., Lin, M., Huang, W., Liu, Q., Chen, H. The effect of modified carbon-doped boron nitride on the mechanical, thermal and γ-radiation stability of silicone rubber composites. *Polymer Degradation and Stability*, *218*(4): 110542, 2023.

[40] Wu, S., Ladani, R.B., Zhang, J., Bafekrpour, E., Ghorbani, K., Mouritz, A.P., Kinloch, A.J., Wang, C.H. Aligning multilayer graphene flakes with an external electric field to improve multifunctional properties of epoxy nanocomposites. *Carbon*, *94*: 607–618, 2015.

[41] Li, X., Mu, Z., Song, X. Microstructure and stress evolution of W nanofilms prepared by arc ion plating under different deposition time and substrate bias. *Journal of Materials Science*, *59*(40): 19254–19272, 2024.